metals

MDPI

Article

Investigation of Oxide Thickness on Technical Aluminium Alloys—A Comparison of Characterization Methods

Ralph Gruber [1], Tanja Denise Singewald [1], Thomas Maximilian Bruckner [1], Laura Hader-Kregl [1], Martina Hafner [2], Heiko Groiss [3], Jiri Duchoslav [4] and David Stifter [4,*]

[1] CEST—Centre for Electrochemistry and Surface Technology, Viktor-Kaplan Str. 2, 2700 Wiener Neustadt, Austria; ralph.gruber@cest.at (R.G.); tanja.singewald@cest.at (T.D.S.); thomas.bruckner@cest.at (T.M.B.); laura.hader-kregl@cest.at (L.H.-K.)
[2] AMAG Rolling GmbH, Lamprechtshausener Str. 61, 5282 Ranshofen, Austria; martina.hafner@amag.at
[3] Christian Doppler Laboratory for Nanoscale Phase Transformations, Center for Surface and Nanoanalytics, Johannes Kepler University Linz, Altenberger Str. 69, 4040 Linz, Austria; heiko.groiss@jku.at
[4] ZONA—Center for Surface and Nanoanalytics, Johannes Kepler University Linz, Altenberger Str. 69, 4040 Linz, Austria; jiri.duchoslav@jku.at
* Correspondence: david.stifter@jku.at

Abstract: In this study the oxide layer of technical 6xxx aluminium surfaces, pickled as well as passivated, were comparatively investigated by means of transmission electron microscopy (TEM), Auger electron and X-ray photoelectron spectroscopy (AES, XPS), the latter in two different operating modes, standard and angle resolved mode. In addition, confocal microscopy and focused ion beam cutting were used for structural studies of the surfaces and for specimen preparation. The results illustrate in detail the strengths and weaknesses of each measurement technique. TEM offers a direct way to reliably quantify the thickness of the oxide layer, which is in the range of 5 nm, however, on a laterally restricted area of the surface. In comparison, for AES, the destructiveness of the electron beam did not allow to achieve comparable results for the thickness determination. XPS was proven to be the most reliable method to reproducibly quantify the average oxide thickness. By evaluating the angle resolved XPS data, additional information on the average depth distribution of the individual elements on the surface could be obtained. The findings obtained in this study were then successfully used for the investigation of the increase in the aluminium oxide thickness on technical samples during an aging test of 12 months under standard storage conditions.

Keywords: technical aluminium alloy; aluminium oxide thickness; oxide thickness characterization; method comparison; X-ray photoelectron spectroscopy; Auger electron spectroscopy; transmission electron microscopy; oxide growth; aging test

check for updates

Citation: Gruber, R.; Singewald, T.D.; Bruckner, T.M.; Hader-Kregl, L.; Hafner, M.; Groiss, H.; Duchoslav, J.; Stifter, D. Investigation of Oxide Thickness on Technical Aluminium Alloys—A Comparison of Characterization Methods. *Metals* **2023**, *13*, 1322. https://doi.org/10.3390/met13071322

Academic Editor: Wangping Wu

Received: 3 July 2023
Revised: 20 July 2023
Accepted: 21 July 2023
Published: 24 July 2023

1. Introduction

Due to global CO_2 emission regulations and the general phase-out of fossil fuels, car manufacturers tend to use more and more lightweight materials to fulfil the required environmental objectives. The change to lighter materials helps to reduce fuel consumption and gives new opportunities in technical applications and design concepts [1–3]. Over the last decades aluminium has been one of the most promising materials for the automotive industry. With a material density about 65% lower than steel, the main advantage is to be found in weight reduction [4]. However, aluminium—especially high-strength alloys—also satisfies the torsion and stiffness requirements for automotive applications and provides outstanding shock absorbing properties which helps to increase passenger safety [2].

Based on the above introduced reasons, structural adhesive bonding for joining car body parts has been established by the automotive industry [5]. This bonding technique, also in combination with other joining methodologies, shows significant advantages in crash performance, cost effectiveness and in the ability of multi-material approaches in

lightweight constructions of automobiles [6]. The most widely used types of structural adhesives for automotive applications are epoxies. These cross-linked polymers are bonding to the aluminium surface and build strong adhesive joints. The long-term durability of those is highly dependent on the surface chemistry of the aluminium substrate prior to bonding—hence the characterization of the top surface layers is of considerable technological importance [4]. Especially, the thin amorphous γ-Al_2O_3 phase on the surface of aluminium and its alloys has a significant effect on the corrosion resistance, wettability and adhesion performance and therefore has often been studied for a better understanding of the relationship between composition and thickness of the aluminium oxide layer and the resulting bonding performance [7–11].

Routinely, oxide thicknesses can be determined using closely industry-related measurement techniques, in particular glow discharge optical emission spectroscopy (GDOES) or infrared reflection absorption spectroscopy (IRRAS). Both methods are established analysis methods for oxide layer thicknesses and are mainly used where corresponding layer thicknesses over 100 nm are required [12]. However, a comparison carried out by us in advance of the current study showed that both techniques, despite being well established methodologies in their field of application, are unsuitable for a reliable determination of aluminium oxide thicknesses below 10 nm.

A technique to characterize aluminium oxide layers in the range of only a few nanometres in thickness is X-ray photoelectron spectroscopy (XPS). The calculation of the oxide thickness can be performed by considering an equation proposed by Strohmeier, which uses the ratio of the measured Al 2p oxide to metal peak intensities [13]. Providing a similar information depth as XPS (i.e., approximately 10 nm), Auger electron spectroscopy (AES) can also be applied for the oxide thickness determination using the evaluation according to Strohmeier due to a comparable energy range of the electrons. In contrast, the quantification of aluminium oxide thicknesses by high resolution images using transmission electron microscopy (TEM) is often performed on a highly localized scale to provide a validation of the values obtained with other characterization techniques [14–16].

Considering the significant effect of an aluminium oxide surface layer on different application properties and the importance of the exact compositional characterization, the question arises, which of the above-mentioned techniques is a valid method for oxide thickness determination on industrial 6xxx aluminium alloys. For this purpose, a comparison was carried out by means of XPS, AES and TEM. Moreover, XPS was taken to quantify the surface chemistry of the aluminium substrates in detail, while TEM was used to describe the top surface layer structure. The resulting oxide thicknesses show a dependency on the chosen method. Consequently, it is necessary to weigh up the advantages and disadvantages of each method for a meaningful characterization of the surface oxide layer.

The findings were then applied to reliably determine the thickness increase in oxide layers on technical aluminium surfaces in an aging study by storing the samples over a period of 12 months under ambient conditions.

2. Materials and Methods

2.1. Materials

As representatives for technical aluminium surfaces used by the automotive industry, an AA 6016 AlMgSi alloy with two different commercial surface finishes was provided by AMAG Austria Metall AG (Ranshofen, Austria). The primary surface treatment was based on automotive standards. In detail, after the finishing annealing, the substrate surface was cleaned by means of acid pickling and a subsequent washing process. After this, the surface was textured using electrical discharge texturing (EDT). A second type of sample experienced a further passivation step with a commercial conversion coating after the cleaning and before surface texturing. Table 1 gives an overview of the sample types used (A1, A2) with the differently applied surface treatments.

Table 1. Overview of investigated sample types and their different surface treatments.

Label	Alloy	Composition	Surface Treatment Procedure	Surface Texture
A1	AA6016	Al98Mg0.6Si1.4	pickling and cleaning	EDT
A2	AA6016	Al98Mg0.6Si1.4	pickling, cleaning and passivation	EDT

2.2. Sample Preparation

Using a metal plate shear the aluminium samples were cut down into pieces with dimensions of 6 × 6 mm^2, 12 × 12 mm^2 or 20 × 20 mm^2, depending on the used characterization method. Prior to analysis, the surfaces of the specimens were cleaned by a three-step ultrasonic degreasing procedure, using different organic solvents, namely aceton (≥99.0% Ph. Eur., VWR Chemicals, Radnor, IN, USA), tetrahydrofurane (THF, ≥99.0% ACS reagent grade, contains 250 ppm BHT as inhibitor, Sigma-Aldrich, St. Louis, MO, USA) and isopropanol (≥99.5% ACS reagent grade, Sigma-Aldrich, St. Louis, MO, USA). The samples were put into a 100 mL beaker, filled with approximately 40 mL of one of the three different solvents and put into an ultrasonic bath for 30 min each.

2.3. Instrumentation

As the analysis method with highest lateral resolution in this comparative study, TEM provides the means to directly measure the oxide thickness in a quantitative way, however, confined to a rather small local area. Therefore, the TEM results were used as reference for the thickness evaluation by choosing representative regions on the sample surfaces. For that purpose, focused ion beam (FIB) cutting in a 1540XB Crossbeam system (Zeiss, Oberkochen, Germany) was used as a preparation method to obtain appropriate specimens for TEM analysis. With gallium ions at 30 keV, lamellae were cut out of the sample surfaces and afterwards thinned to electron transparency. Prior to FIB preparation the surface of the samples were protected by an electron stimulated platinum deposition to avoid damaging the oxide layer during the subsequent preparation steps. The positions from where the lamellae were cut out were chosen after an investigation of the surface structure, roughness and texture using a MarSurf CM mobile confocal microscope (Mahr GmbH, Göttingen, Germany). To measure the oxide layer thickness, TEM measurements were performed in a JEM-2200FS system (JEOL, Akishima, Japan), using an accelerating voltage of 200 kV. The high-resolution TEM images were recorded by means of zero-loss filtering, using the in-column Ω-filter. The TEM system is additionally equipped with an energy-dispersive X-ray detector (EDX) from Oxford Instruments (Abingdon, UK) for elemental analysis using the microscope in the scanning mode (STEM).

Providing different measurement modes, XPS was chosen to be a much faster and more versatile method which provides complementary data. Next to an overview of the elemental and chemical composition of the surface layers, XPS was mainly used to obtain the oxide thickness. All measurements were performed using a Thetaprobe XPS system (Thermo Scientific, Waltham, MA, USA). The device features a monochromatic Al K_α X-ray source ($h\nu$ = 1486.6 eV) and is equipped with a dual flood gun for surface charge neutralization. The spot size of the X-ray beam was chosen to be 400 µm in diameter in order to obtain an average oxide layer thickness. To exploit the whole data potential of this analysis technique the XPS measurements were performed in standard as well as in angle resolved mode. For each mode, survey spectra were obtained using 200 eV as pass energy with an energy step width of 1 eV. More detailed high resolution (HR) spectra were recorded with a pass energy of 50 eV and 0.05 eV step width. The evaluation of the XPS data was performed using the Avantage software package from the system supplier.

As AES is also sensitive to the same surface near region as XPS, a scanning AES microscope (JEOL JAMP 9500F, Akishima, Japan) was additionally used to determine the oxide layer thickness. For spectroscopy of Auger electrons, the device is equipped with a hemispherical electron energy analyser and a channeltron detector, positioned at an angle

of 60° with respect to the beam direction of the electron gun. As the AES microscope can record images using secondary and backscatter electron detectors the system was also applied to determine the microstructure of the textured aluminium surface. The investigations were carried out with the sample surface perpendicular to the electron beam using 10 kV accelerating voltage and a beam current of 10 nA.

3. Results

For the comparison of the different measurement techniques with respect to their performance in obtaining the oxide thickness, it was necessary to define a reference value for each sample. The commercial aluminium alloy with the two different types of surface treatment was investigated, at first, by means of TEM. Due to the complex EDT pattern on the surfaces the positioning for the FIB preparation was crucial to quantify the oxide thickness in a representative way for the (majority of) the surface. Figure 1 shows the EDT structured surface of the pickled aluminium sheet of type A1 observed by confocal microscopy.

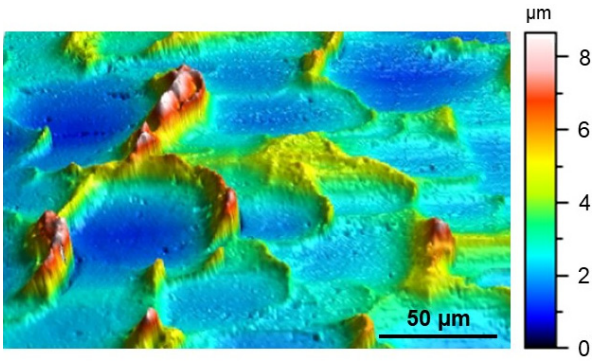

Figure 1. EDT surface structure of a pickled specimen of type A1 investigated by confocal microscopy.

The imprints result from the rolling process and lead to an average surface roughness of R_a = 0.65 µm. Due to high shear forces during the rolling process the edges of the EDT craters often show distinctly different microstructure compared to the flatter regions, which account for the largest portion of the surface area. In addition, rolling and texturing affects the local surface properties due to the mechanical displacement during the production procedure and is often described as a surface near deformed layer (NSDL) [17–19]. As shown in Figure 2 the positions for the FIB preparation of the lamellae were chosen to be in a flatter and homogeneous area of the sample. This guarantees a rather uniform oxide layer without influences of the extreme surface texture or the NSDL on the ridges caused by the production process.

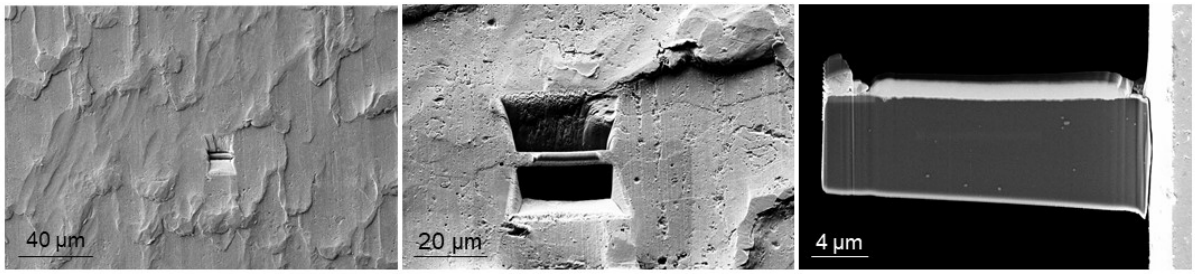

Figure 2. Position and preparation steps of a TEM lamella using FIB cutting and thinning.

3.1. Reference Value from Transmission Electron Microscopy

To obtain representative values for a comparison of the methods the oxide layer thickness was measured from TEM images similar to the one presented in Figure 3. A section of a lamella of sample type A1 with a clearly visible uniform oxide layer on top of the aluminium bulk is shown. The darker area in the image represents the sputter-coated platinum layer which avoided damage to the oxide layer during FIB preparation. It can

be clearly differentiated from the brighter and grey coloured aluminium oxide layer. For better statistical and representative oxide thickness values, the measurement was carried out at least five times at different sections on a lamella for each sample type.

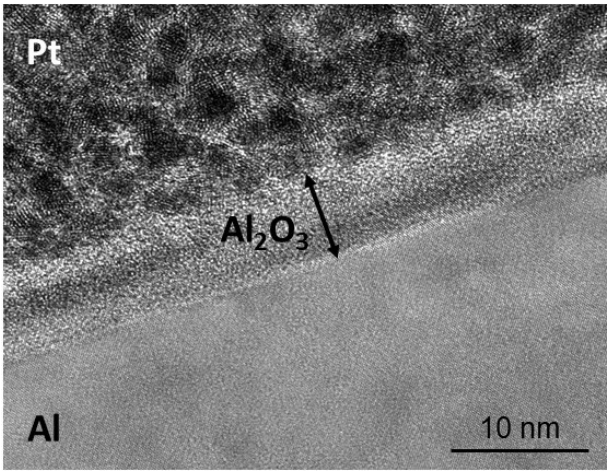

Figure 3. Presence of a uniform oxide layer on a subsection of a lamella of type A1.

Since the production process of the two sample types differs only by one additional passivation step without any further rise in temperature, the expected oxide layer thicknesses for both types should be in the same nanometre range. The obtained average oxide layer thicknesses for both types, given in Table 2, confirms this assumption.

Table 2. TEM results of the oxide layer thicknesses.

Sample	Av. Oxide Layer Thickness [nm]
A1	5.8 ± 0.6
A2	5.6 ± 0.3

EDX-mappings were additionally performed on sections of the lamellae, exhibiting a difference in the layer structure between the pickled and the additional passivated sample types. As shown in Figure 4, sample type A1 differs from A2 due to the presence of a non-uniform conversion layer. The aluminium bulk (light blue) is fully covered by an oxide layer (green). For A2 titanium (red), which is part of the conversion coating, is visibly deposited on top of the oxide in a non-uniform way. The peninsular-like growth of the zirconium and titanium-based conversion layer is electrochemically driven. In detail, during the initial stages of the coating process the oxide layer experiences a dissolution due to the fluoride containing coating solution. The surface near intermetallic phases becomes more cathodic, which in turn favours the formation of a conversion layer in the region surrounding those phases [20].

3.2. XPS

After the fundamental characterization by TEM, all sample types were investigated using XPS in two different operation modes, standard as well as angle resolved, for oxide thickness determination. Compared to the spatially restricted local analysis provided by TEM, XPS offers the advantage of being a much faster and laterally averaging method which is more suitable for the characterization of technical sample surfaces. Consequently, the X-ray beam size for both analysis modes was chosen to be 400 µm in diameter. In addition, XPS does not require tedious sample preparation steps prior analysis and is nearly non-destructive, in contrast to AES, as presented later in this study [21].

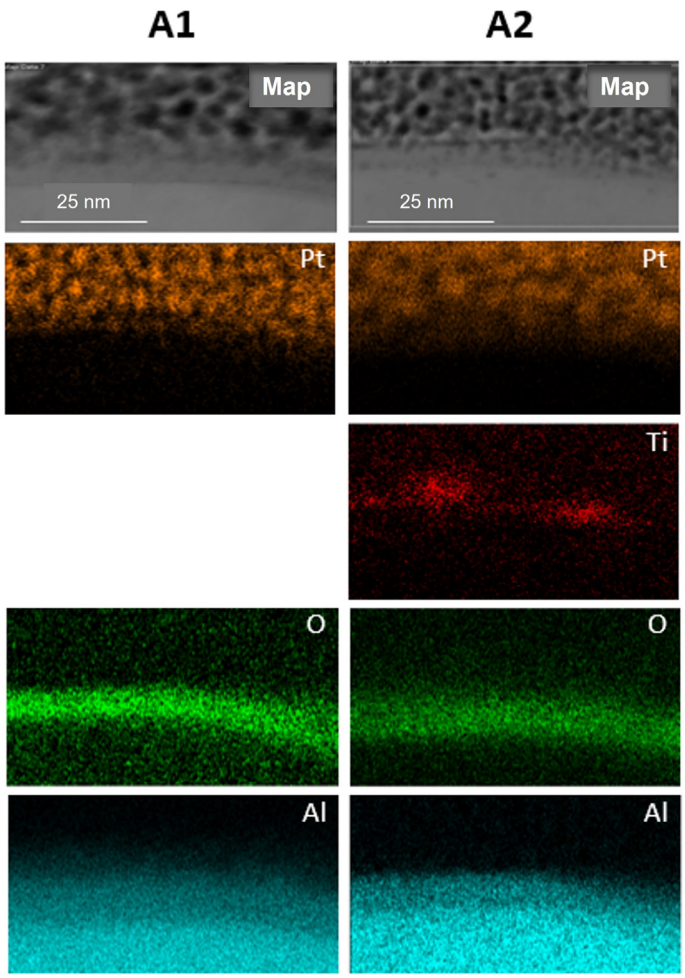

Figure 4. Layer structure comparison of both sample types by EDX elemental mapping.

At first, standard mode XPS was used to obtain an overview of the elemental composition of the topmost surface layer of all surface treated aluminium samples. The comparison of the survey spectra shown in Figure 5 reveals the difference of the surface chemistry due to the different pre-treatment procedures. Despite the three-step cleaning procedure with organic solvents, all samples revealed carbon contamination with a concentration around 30 at.% on the surfaces. In addition, also other contamination elements, e.g., Na, S and Ca could be detected on the analysed surfaces in negligible traces under 1 at.%. By omitting these contaminations, a general elemental surface composition could be evaluated as summarized in Table 3. Comparing the major constituents of the samples, it was found that Al, O and C are the dominating elements present on the surfaces, closely followed by F with varying concentrations, depending on the pre-treatment process. The high carbon contamination content at the samples surface, partly bound to oxygen, could be a reason for the difference in the determined stoichiometry of the Al_2O_3 oxide, as shown in Table 3. The fluorine concentration of the non-passivated aluminium alloy of type A1 can be attributed to the fluorine-containing ingredients of the pickling bath. Most of the detected fluorine as well as all of titanium and zirconium on the passivated sample type A2 originate from the conversion coating.

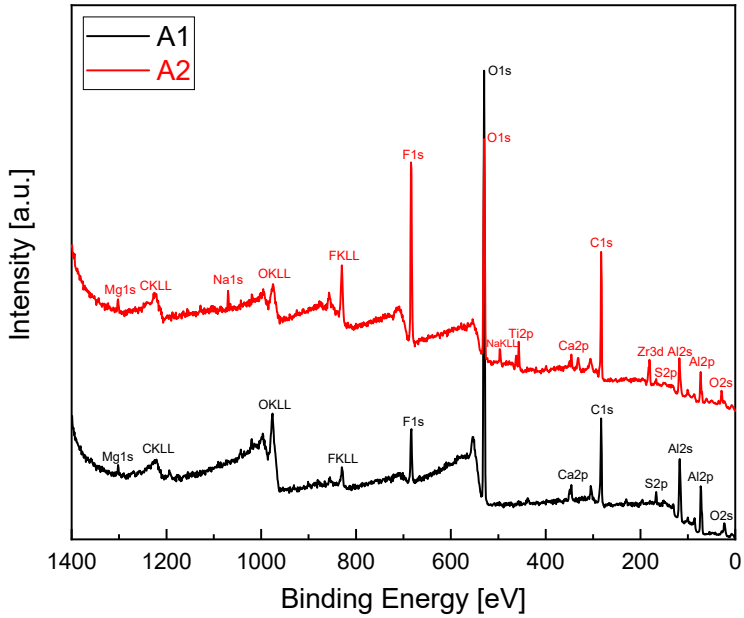

Figure 5. Comparison of XPS survey spectra of both sample types.

Table 3. Elemental composition of the surface layer on all analysed samples obtained by XPS.

Sample	Elemental Composition [at.%]						
	Al	**O**	**C**	**F**	**Mg**	**Ti**	**Zr**
A1	19	38	31	5	0.4		
A2	16	29	32	18	0.6	1.4	1.1

To better identify the chemical components in the topmost surface layers, HR spectra of the major elemental constituents, aluminium, oxygen, fluorine and carbon for sample type A1, and additional titanium and zirconium for sample type A2, were additionally recorded. From the results of the HR data, it was derived that the sample surfaces are homogeneous in terms of chemical composition and only differ due to their very own pre-treatment history. The bulk aluminium alloy, which predominantly consists of aluminium without any significant alloying element contents in the topmost surface areas, is covered by an Al_2O_3 layer on all samples. Pickled specimens show small amounts of fluorine, which originates from components of the pickling bath solution, embedded into the oxide layer. On the passivated samples fluorine could equally be detected within the oxide layer, although, in much higher concentrations. In combination with titanium and zirconium on top of the oxide this result, as mentioned above, is attributed to the conversion coating process during production. As already seen from the survey spectra, carbon was detectable on both surfaces despite an intense cleaning procedure. By fitting the high-resolution spectrum of the C1s core level three different carbon peaks could be identified (C-C/H, C-O, C=O), which are mostly attributed to different components of the lubricants which are used during the rolling process of the aluminium sheets for automotive applications.

The above findings are based on HR spectra, which were taken in the angle resolved mode of the XPS. This AR data was used, in addition to the identification of chemical composition in the topmost surface layers, to also qualitatively estimate the depth distribution of the major elemental constituents. By taking the negative logarithm of the peak intensity ratio collected at bulk- and surface-sensitive angles, as shown in Figure 6, an average relative depth position for each element can be obtained. These relative depth plots do not have a quantitative depth-axis since the absolute depth position is not derived by this method. However, these plots qualitatively indicate the order of the different elemental species with respect to each other [22,23].

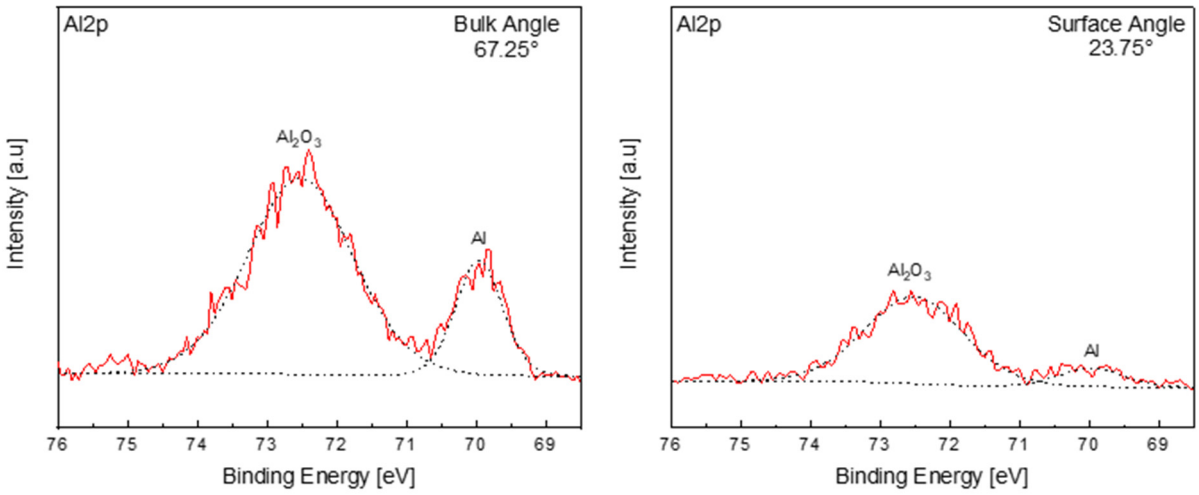

Figure 6. ARXPS surface and bulk angle HR spectra of Al2p.

In Figure 7a the relative depth position of each surface related element of sample type A2 is shown. The carbon contamination originates from the topmost surface region, whereas the signals of the major elemental constituents of the conversion coating, i.e., Zr, Ti, F and O, come from the intermediate information depth range of this method. The aluminium oxide layer is also found in the middle depth region directly beneath the conversion coating. The signals of alloying elements such as aluminium, magnesium and silicon originate from larger depths within the total information depth range of ARXPS and are allocated towards the bulk section of the sample. In addition to the determination of relative depth positions of different elements, ARXPS provides the means to obtain even full in-depth concentration profiles in a non-destructive way. In Figure 7b the corresponding virtual depth profile from sample type A2 is depicted. The findings reflect the results of the relative depth plot and confirm the layered structure as observed in the TEM analysis. The elements originating from the passivation step are located on top of the aluminium oxide layer and are covered by carbon contaminations. Alloying elements such as magnesium and silicon can be found again towards the aluminium bulk section.

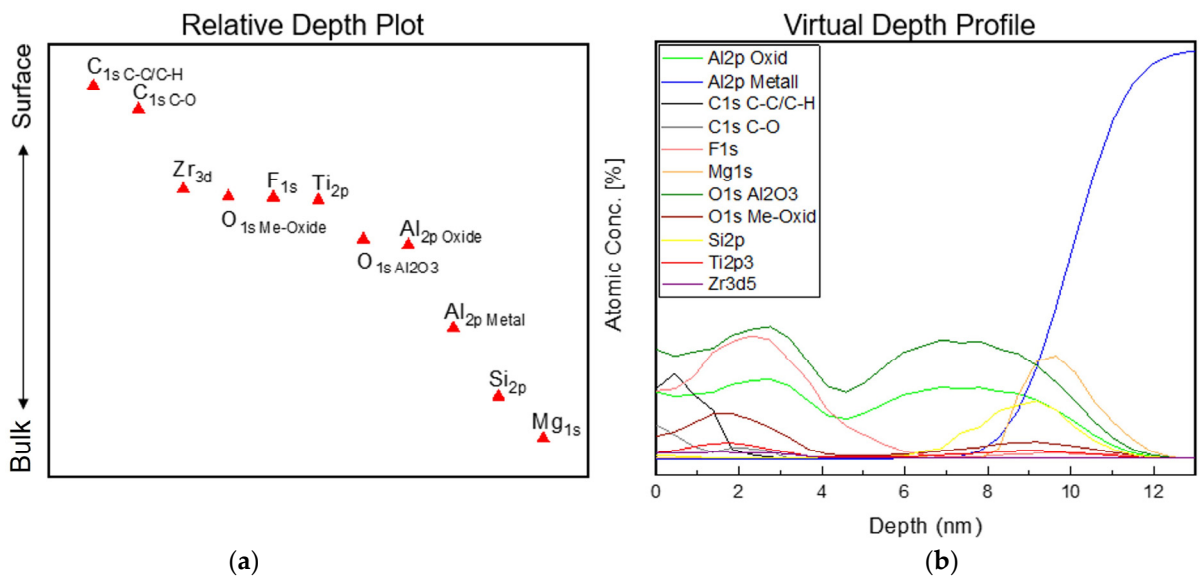

Figure 7. (**a**) Relative depth plot (**b**) Corresponding virtual depth profile. Both obtained by ARXPS.

Next to an overview of the elemental and chemical composition of the surface layers, XPS was mainly used to obtain the oxide thickness. The calculation method is based on the

Beer-Lambert law and has been introduced by Strohmeier [13]. The equation, shown in Equation (1), covers the ratio of the measured Al2p oxide to metal peak intensities with respect to the elemental inelastic mean free paths (IMFP) λ_m and λ_o, the atomic volume densities N_m and N_o as well as the average take off angle θ and can be applied for true oxide layer thicknesses < 10 nm.

$$d_{oxide}\left(\text{Å}\right) = \lambda_o \sin\theta ln\left(\frac{N_m \lambda_m I_o}{N_o \lambda_o I_m} + 1\right) \quad (1)$$

The volume density ratio of aluminium atoms in metal to oxide used in this study was N_m/N_o = 1.5. Furthermore, the average take off angle was θ = 60° and for the IMFP values in metallic aluminium λ_m = 26 Å and in Al_2O_3 λ_o = 28 Å was used [13,24]. In consideration of the given parameters the aluminium oxide thickness was calculated using the Al2p HR spectra from both, standard as well as angle resolved mode. The corresponding intensities I_m and I_o were obtained by fitting the peak with a higher binding energy as Al_2O_3 (Al2p oxide) and the other at lower binding energy as metallic aluminium (Al2p metal). Compared to the values obtained by TEM, the results of the standard XPS measurement in Table 4 are close, but show slightly lower oxide thicknesses. The underestimation of the thickness is, besides in the limitation of the Strohmeier model, due to the fact that the chosen spot size of the X-ray beam is averaging the results in the observation area. Aside from that of the XPS technique itself, in angle resolved or standard mode, it has little to no effect on the results when performing the thickness calculation based on the Strohmeier equation. This can be explained by the evaluation procedure. In order to obtain the corresponding Al2p spectra out of the AR data, one has to collapse every spectrum from each measured angle to obtain one single main spectrum. This main Al2p spectrum differs hardly from the spectrum as obtained by standard mode XPS measurements.

Table 4. Results of oxide thickness evaluation by different XPS-based methods.

Sample	Oxide Thickness Standard Mode [nm]	Oxide Thickness AR-Overlayer [nm]	Oxide Thickness Virtual Depth Profile [nm]
A1	4.7 ± 0.1	4.1 ± 0.1	6.2 ± 0.6
A2	4.9 ± 0.2	4.3 ± 0.2	6.5 ± 0.8

Aside from the oxide thickness calculation based on the procedure proposed by Strohmeier, ARXPS provides an overlayer thickness calculation procedure implemented in the Avantage software package of the system manufacturer. The calculation is based on all of the generated AR data (and not only on a collapsed single spectrum) and requires additional information about material properties, i.e., chemical formula, density and bandgap in order to obtain the corresponding IMFPs for the thickness calculation. The results of this evaluation, taking the single HR AR spectra into account, are given in Table 4 (named AR-Overlayer).

A further possibility for the determination of the oxide thickness is based on virtual depth profiles from ARXPS data as shown in Figure 7 for sample type A2. The oxide thickness can be derived from the Al2p oxide signal with respect to the reconstructed depth-axis. The results of this evaluation are also shown in Table 4. The obtained values indicate that the depth axes in virtual depth profiles from ARXPS has to be taken with care and that an analysis of the oxide thickness in a quantitative way is not straight forward, especially on technical aluminium alloys. However, such an AR-based evaluation complements the elemental and chemical surface characterization by standard XPS analysis and is a valuable technique to reveal the existing layer structure on industrial aluminium surfaces.

3.3. AES

Providing a similar information depth as XPS from the same surface near region AES was chosen to be the third method for this comparative study. Due to the same range of electron energies, identical IMFP values for aluminium and its oxide as for XPS can be used and the determination of the oxide thickness using the equation after Strohmeier (Equation (1)) is applicable. Consequently, all samples were evaluated using the first derivative of the fitted high resolution aluminium spectra, such as the one shown in Figure 8. The main advantage of using the first derivative of measured AES spectra is the background suppression. The ratio of the measured aluminium oxide to metal peak intensities, which are necessary for the application of Equation (1), were calculated using the difference of the minimum and maximum points from each compound peak structure. All spectra were fitted equally by means of a linear combination fit. For that purpose, acquired spectra of pure reference materials, metallic aluminium and Al_2O_3, were used in combination to fit the spectra of the samples. This procedure generates a reproduceable way to qualitatively evaluate high resolution AES measurements.

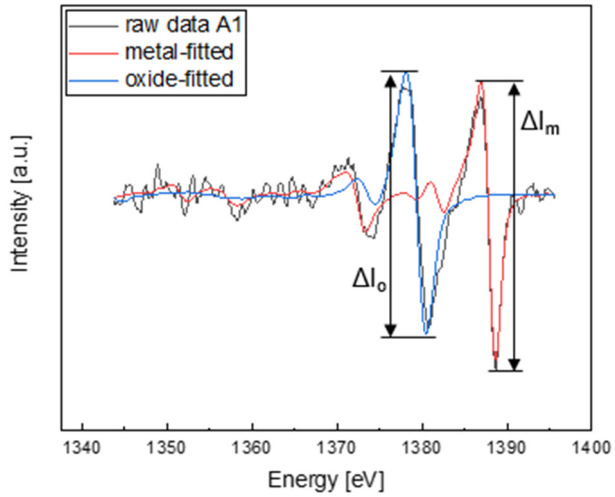

Figure 8. AES high resolution Al spectrum with fitted components.

As mentioned above, the usage of focused electron beams can lead to a degradation of metallic oxides [21]. This observation was also made in the current study when performing point measurements on all samples. As shown in Figure 9, HR spectra were additionally recorded using area measurements instead of point measurements in order to decrease degradation effects. By stepwise doubling the field of investigation the influence of different measurement areas on the oxide thickness values was obtainable. The areas were positioned in the flatter zones of the EDT surface to reliably quantify the oxide thickness. The findings given in Table 5 clearly demonstrate the degradation effect of the electron beam depending upon the resulting beam exposure. The average oxide thickness of sample type A1 obtained using point measurements is more than three times less than the average acquired by area investigations. The increase in the measured area also involves an increase in the thickness of the investigated oxide layer. Comparing a measurement area four times the size as the initial one, the increase in oxide thickness is approximately 46%.

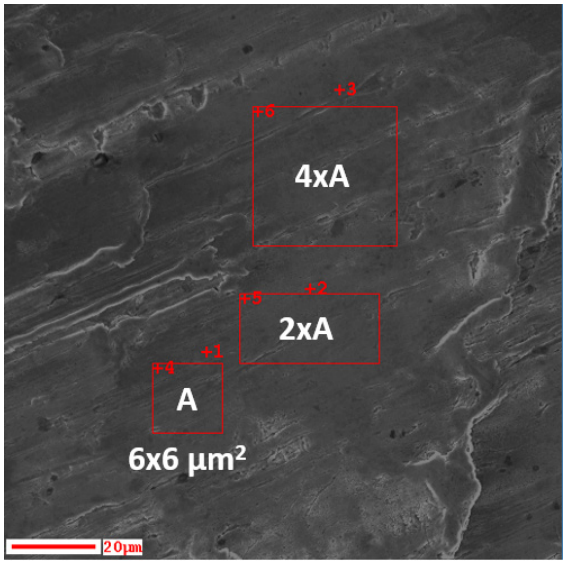

Figure 9. Observation area during AES measurements.

Table 5. Comparison of obtained thickness values for point and area AES measurements.

Sample	Measurement Point/Area	Oxide Thickness [nm]	Mode
A1	1–3	0.69	Point
	4	2.11	Area A
	5	2.60	Area 2A
	6	3.10	Area 4A

4. Discussion

To further elucidate which method is the most practical one for a reliable determination of the oxide thickness on technical aluminium alloys, the overall results are compared in Figure 10. TEM provides the highest lateral resolution. Although this method offers the best way to reliably quantify the oxide thickness, it should be considered that the results are referred only to a very confined region of the real samples surface. To obtain statistical validity of the measurement data, more different measurement positions evenly distributed on the surface are recommended to draw reliable conclusions about the average oxide thickness of the investigated samples. TEM is also not practicable for quick analysis due to laborious sample preparation procedures. Nevertheless, the results of the TEM analysis in this study show that all investigated sample types have a similar oxide thickness despite different treatment processes, namely the additional passivation step of sample type A2 has no significant effect on the thickness of the initial oxide layer.

Comparing the results of the two different modes for XPS measurements, oxide thickness values from the standard mode differ only slightly from the values obtained by AR mode. However, the thickness determination from virtual depth profiles seems to show significantly higher values as compared to the so-called overlayer model and the calculation according to Strohmeier. This discrepancy can be explained by inaccuracies of input parameters needed for generating such virtual depth profiles, as well as by limitations of the underlying model for reconstructing the profile out of the ARXPS data. There are several factors, e.g., the indication of the correct chemical composition of the different surface compounds, which have an influence on the results. Nevertheless, by providing the opportunity to obtain information about elemental and chemical surface composition and additionally about the average depth distribution of different elemental species and the layer structure (e.g., in relative depth plots), the angle resolved mode is generally preferred. Comparing the XPS results to the TEM ones, a small discrepancy in the range of less than a

nanometre occurs. This difference is attributed to a combination of several factors. Firstly, standard curve fitting of the metallic Al2p main peak was proven to have an error in the percentage range. This discrepancy originates from an overestimation of contributed substrate photoelectrons to the inelastic background [24]. Furthermore, XPS is a much more averaging method as compared to the highly localized investigation by TEM. Since the investigated samples originate from industrial production and exhibit a surface texture with a certain roughness, local oxide thickness deviations may exist. In addition, the TEM lamellae, in the size of approximately 20 µm, were prepared from the flatter areas of the EDT imprints, giving values without influences from the surface texture, especially from the ridges and the deformed microstructure at the edges of the EDT imprints [17–19,24]. With an average spot size of 400 µm in diameter XPS is sensitive to every part of the textured aluminium surface. Hence, the values of the oxide thickness obtained by XPS may give the most relevant overall picture for technical aluminium surfaces.

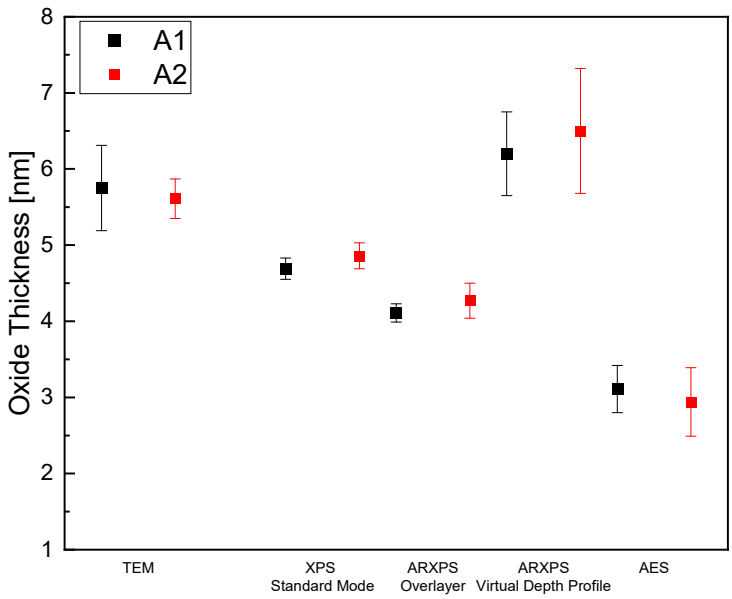

Figure 10. Comparison of obtained Al_2O_3 thickness values by different measurement methods.

Finally, the destructiveness of the focused electron beam during AES measurement becomes apparent in the results. Especially point measurements show a significant degradation of the oxide layer. Thus, area measurements were chosen to suppress and overcome degradation to a certain degree. The smallest possible area for the given magnification was 6×6 µm^2, which led to a less destructive interaction with the oxidic surface. Hence, the measured oxide thickness increased by a factor of three with respect to point measurements. Nevertheless, the resulting oxide layer still deviates significantly from the TEM and XPS results. Therefore, the measurement area was increased stepwise up to 12×12 µm^2, resulting in an improvement, but being still far below the values obtained by the other methods. Nevertheless, AES can act as a link between the nanoscopic view of TEM and the laterally averaging one of XPS, when taking degradation into account.

Based on our findings, the increase in the aluminium oxide thickness over time was observed during aging for one year at standard storage conditions. The results obtained by XPS were compared again with those by TEM, since these methods are the most accurate ones, and are shown in Figure 11. As known from the literature, the growth rate of aluminium oxide at ambient pressures and temperatures is initially extremely rapid and decreases with increasing thickness of the oxide. In general, the growth rate is positively influenced by increased temperatures to a certain point and elevated oxygen concentrations [25]. However, as soon as a so-called limiting thickness is reached, the oxide growth stops and does not change with time [26]. The aluminium oxide of the investigated 6xxx

alloy also follows this trend. It seems that the limiting thickness is reached already before half a year of aging for both sample types. It shall be noted that the initial difference in the obtained oxide thickness between the two analysis methods, XPS and TEM, could also be detected again after one year of aging for both samples. Of especial importance is the gained knowledge that XPS underestimates TEM data by approximately one nanometre. Consequently, aluminium oxide layer determination by means of XPS is a reproducible and representative, as well as a relatively easily to be performed method for the characterization of technical aluminium surfaces.

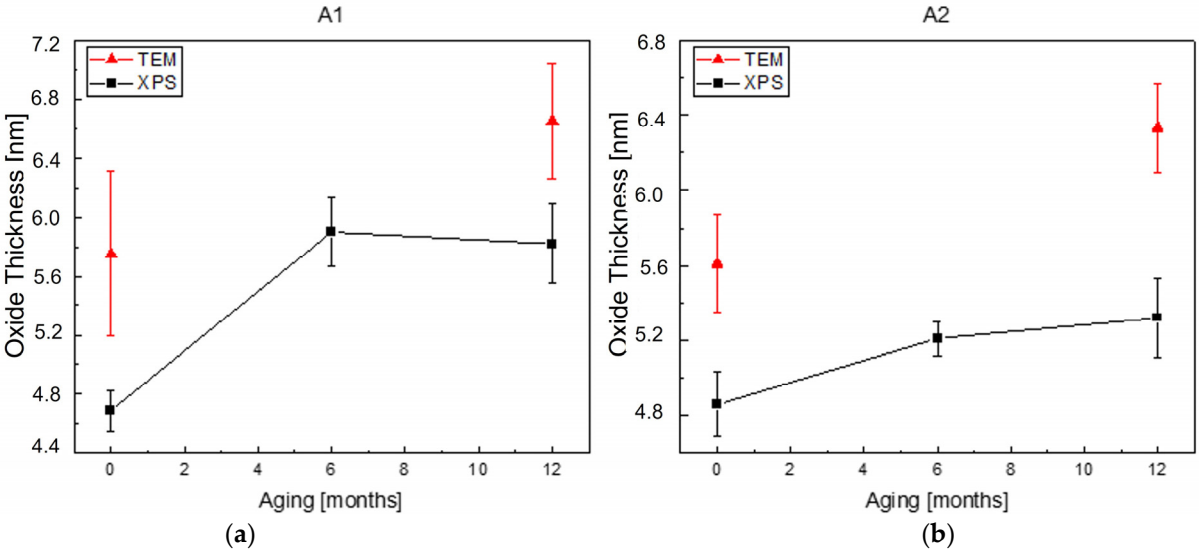

Figure 11. Increase in the aluminium oxide thickness over time during aging at standard storage conditions for one year observed by means of XPS and TEM. (**a**) shows results of sample type A1, (**b**) refers to sample A2.

5. Conclusions

In this comparative study, a valid and reliable method for oxide thickness determination on an industrial 6xxx aluminium alloy was searched for. The oxide thicknesses were determined by means of TEM, XPS—in two different operating modes, standard and angle resolved mode—as well as by AES.

(1) The results show that XPS gives reproducibly accurate averaged values of the thickness and provides even the possibility to generate information about elemental and chemical surface composition and additionally provides information about the average depth distribution of different elemental species and the resulting layer structure.
(2) Although TEM offers the highest lateral resolution and therefore the most direct and accurate way for oxide thickness quantification, it should be considered that the results are referred only to a rather confined region of the real samples surface. Reliable conclusions based on TEM measurements require statistical validity by accessing multiple measurement positions evenly distributed on the samples surface. Furthermore, sample preparation for TEM investigations requires significantly higher experimental effort as compared, e.g., for XPS.
(3) In this study, AES acted as a link between the nanoscopic view of TEM and the laterally averaging characteristics of XPS. However, the destructiveness of the focused electron beam during AES measurements becomes apparent in the results, where a significant degradation of the oxide layer was detected.
(4) Finally, an aging test at standard storage conditions proved that the aluminium oxide layer determination by means of XPS is reproducible and in combination with a short measurement time and minimal sample preparation requirements, a highly suitable method for the characterization of technical aluminium surfaces. This work further clearly illustrates the importance of knowing the individual characteristics

and strengths of each measurement technique, especially when performing industry related applied research.

Author Contributions: Conceptualization, R.G. and D.S.; methodology, D.S. and H.G.; formal analysis, J.D., T.D.S. and T.M.B.; investigation, R.G.; resources, M.H. and D.S.; data curation, R.G.; writing—original draft preparation, R.G.; writing—review and editing, D.S.; supervision, L.H.-K., M.H. and D.S.; project administration, L.H.-K. and M.H.; All authors have read and agreed to the published version of the manuscript.

Funding: The Comet Centre CEST is funded within the framework of COMET—Competence Centers for Excellent Technologies by BMVIT, BMDW as well as the Province of Lower Austria and Upper Austria. The COMET programme is run by FFG. This work originates from research in the Durabond and GreenMetalCoat (FFG 865864, Comet-Center (K1), 2019–2022; FFG 899594, Comet-Center (K1), 2023) projects.

Data Availability Statement: Not applicable.

Acknowledgments: J.D. and D.S. acknowledge the government of Upper Austria for financial support (project ASAES). The financial support by the Austrian Federal Ministy of Labour and Economy, the National Foundation of Research, Technology and Development and the Christian Doppler Research Association is gratefully acknowledged.

Conflicts of Interest: The authors declare no conflict of interest.

References

1. Njuguna, J. *Lightweight Composite Structures in Transport: Design, Manufacturing, Analysis and Performance*; Elsevier Science: Amsterdam, The Netherlands, 2016.
2. Hirsch, J. Recent development in aluminium for automotive applications. *Trans. Nonferrous Met. Soc. China* **2014**, *24*, 1995–2002. [CrossRef]
3. Crolla, D.; Ribbens, W.; Heisler, H.; Blundell, M.; Harty, D.; Brown, J.; Serpento, S.; Robertson, A.; Garrett, T.; Fenton, J.; et al. *Automotive Engineering e-Mega Reference*; Elsevier Science: Amsterdam, The Netherlands, 2009.
4. Cavezza, F.; Boehm, M.; Terryn, H.; Hauffman, T. A Review on Adhesively Bonded Aluminium Joints in the Automotive Industry. *Metals* **2020**, *10*, 730. [CrossRef]
5. Pana, G.M. Developments of audi space frame technology for automotive body aluminum construction. *Appl. Mech. Mat.* **2020**, *896*, 127–132. [CrossRef]
6. Association, E.A. *EAA Aluminium Automotive Manual—Joining, The Aluminium Automotive Manual*; European Aluminium Association: Ljubljana, Slovenia, 2015; pp. 1–5.
7. Mercier, D.; Rouchaud, J.-C.; Barthés-Labrousse, M.-G. Interaction of amines with native aluminium oxide layers in non-aqueous environment: Application to the understanding of the formation of epoxy-amine/metal Interphases. *Appl. Surf. Sci.* **2008**, *254*, 6495–6503. [CrossRef]
8. Morsch, S.; Liu, Y.; Malanin, M.; Formanek, P.; Eichhorn, K.-J. Exploring wheter a buried nanoscale interphase exists within epoxy-amine coatings: Implications for adhesion, fracture thoughness and corrosion resistance. *Appl. Nano Mater.* **2019**, *2*, 2494–2502. [CrossRef]
9. Wu, G.; Dash, K.; Galano, M.L.; O'Reilly, K.A.Q. Oxidation studies of Al alloys: Part II Al-Mg alloy. *Corros. Sci.* **2019**, *155*, 97–108. [CrossRef]
10. Bechtel, S.; Nies, C.; Fug, F.; Grandthyll, S.; Müller, F.; Possart, W. Thin epoxy layers on native aluminium oxide: Specific ageing processes in mild conditions. *Thin. Solid Films* **2020**, *695*, 137756. [CrossRef]
11. Cornette, P.; Zanna, S.; Seyeux, A.; Costa, D.; Marcus, P. The native oxide film on a model aluminium-copper alloy studied by XPS and ToF-SIMS. *Corros. Sci.* **2020**, *174*, 108837. [CrossRef]
12. Takano, T.; Matsuya, H.; Kowalski, D.; Kitano, S.; Aoki, Y.; Habazaki, H. Raman and glow discharge optical emission spectroscopy studies on structure and anion incorporation properties of a hydrated alumina film on aluminum. *Appl. Surf. Sci.* **2022**, *592*, 153321. [CrossRef]
13. Strohmeier, B.R. An ESCA method for determining the oxide thickness in aluminum alloys. *Surf. Interface Anal.* **1990**, *15*, 51–56. [CrossRef]
14. Suárez-Campos, G.; Cabrera-German, D.; Castelo-González, A.O.; Avila-Avendano, C.; Ríos, J.L.F.; Quevedo-López, M.A.; Aceves, R.; Hu, H.; Sotelo-Lerma, M. Characterization of aluminum oxide thin films obtained by chemical solution deposition and annealing for metal-insulator-metal dielectric capacitor applications. *Appl. Surf. Sci.* **2020**, *513*, 145879. [CrossRef]
15. Din, R.U.; Gudla, V.C.; Jellesen, M.S.; Ambat, R. Accelerated growth of oxide film on aluminium alloys under steam: Part I: Effects of alloy chemistry and steam vapour pressure on microstructure. *Surf. Coat. Tech.* **2015**, *276*, 77–88. [CrossRef]

16. Evangelisti, F.; Stiefel, M.; Guseva, O.; Nia, R.P.; Hauert, R.; Hack, E.; Jeurgens, L.P.H.; Ambrosio, F.; Pasquarello, A.; Schmutz, P.; et al. Electronic and structural characterization of barrier-type amorphous aluminium oxide. *Electrochim. Acta* **2017**, *224*, 503–516. [CrossRef]
17. Liu, E.; Pan, Q.; Liu, B.; Ye, J. Microstructure Evolution of the near-surface deformed layer and corrosion behaviour of hot rolled AA7050 aluminium alloy. *Materials* **2023**, *16*, 4632. [CrossRef] [PubMed]
18. Lunder, O. Chromate-Free Pre-Treatment of Aluminium for Adhesive Bonding. Ph.D. Thesis, Norwegian University of Science and Technology, Trondheim, Norway, 2003.
19. Huttunen-Saarivirta, E.; Heino, H.; Vaajoki, A.; Hakala, T.J.; Ronkainen, H. Wear of additively manufactured tool steel in contact with aluminium alloy. *Wear* **2019**, *202934*, 432–433. [CrossRef]
20. Andreatta, F.; Turco, A.; de Graeve, I.; Terryn, H.; de Wit, J.H.W.; Fedrizzi, L. SKPFM and SEM study of the deposition mechanism of Zr/Ti based pre-treatment on AA6016 aluminum alloy. *Surf. Coat. Tech.* **2007**, *201*, 7668–7685. [CrossRef]
21. Duchoslav, J.; Kehrer, M.; Truglas, T.; Groiß, H.; Nadlinger, M.; Hader-Kregl, L.; Riener, C.K.; Arndt, M.; Stellnberger, K.H.; Luckeneder, G.; et al. The effect of plasma treatment on the surface chemistry and structure of ZnMgAl coatings. *Appl. Surf. Sci.* **2020**, *504*, 144457. [CrossRef]
22. Duchoslav, J.; Arndt, M.; Steinberger, R.; Keppert, T.; Luckeneder, G.; Stellnberger, K.H.; Hagler, J.; Riener, C.K.; Angeli, G.; Stifter, D. Nanoscopic view on the initial stages of corrosion of hot dip galvanized Zn-Mg-Al coatings. *Corros. Sci.* **2014**, *83*, 327–334. [CrossRef]
23. Arndt, M.; Duchoslav, J.; Itani, H.; Hesser, G.; Riener, C.K.; Angeli, G.; Preis, K.; Stifter, D.; Hingerl, K. Nanoscale analysis of surface oxides on ZnMgAl hot-dip-coated steel sheets. *Anal. Bioanal. Chem.* **2012**, *403*, 651–661. [CrossRef]
24. Tanuma, S.; Powell, C.J.; Penn, D.R. Calculations of electron inelastic mean free paths for 31 materials. *Surf. Interface Anal.* **1988**, *11*, 577–589. [CrossRef]
25. Rullik, L.; Evertsson, J.; Johansson, N.; Bertram, F.; Nilsson, J.-O.; Zakharov, A.A.; Mikkelsen, A.; Lundgren, E. Surface oxide development on aluminum alloy 6063 during heat treatment. *Surf. Int. Anal.* **2019**, *51*, 1214–1224. [CrossRef]
26. Cabrera, N.; Mott, N.F. Theory of the oxidation of metals. *Rep. Prog. Phys.* **1949**, *12*, 163–184. [CrossRef]